Journal of Catalysis **182,** 199–207 (1999)
Article ID jcat.1998.2332, available online at http://www.idealibrary.com on IDEAL®

Evaluation of Surface and Bulk Phases during Oxychlorination/ Reduction Cycles of Pt–Re Catalysts

M. Fernández-García,*,[1] F. K. Chong,† J. A. Anderson,† C. H. Rochester,† and G. L. Haller‡

*Instituto de Catálisis y Petroleoquímica, CSIC, Campus Universidad Autónoma, Cantoblanco, 28049-Madrid, Spain; †Department of Chemistry, University of Dundee, Dundee DD1 4HN, United Kingdom; and ‡Department Chemical Engineering, Yale University, 9 Hillhouse Avenue, New Haven, Connecticut 06520

Received July 17, 1998; revised October 16, 1998; accepted November 3, 1998

A 0.3 wt% Pt–0.3 wt% Re/Al_2O_3 catalyst and monometallic 0.3 wt% Pt reference have been studied by X-ray absorption near-edge structure (XANES), hydrogen chemisorption, and *n*-heptane reforming, at stages during a series of oxychlorination/reduction cycles. The initial precalcined, chlorine-free system contains separate Pt^{4+} and Re^{7+} oxide clusters, which are reduced through a Re intermediate, yielding a Pt–Re alloy. Several chemical characteristics of the Re intermediate and the alloyed phase are revealed by the study. Subsequent oxychlorination of the reduced catalysts leads to the disruption of the alloy particles, producing initially Re^{7+} oxide and Pt^{4+} oxychloride species, with the latter eventually losing most of its chlorine ligands to form an oxide-like phase at higher treatment temperatures. The presence of chlorine influences the behavior of the subsequent reduction process, in particular, modifying the final properties of the zero-valent alloyed phase. The physical and chemical parameters affecting the Cl-induced changes are discussed on the basis of the XANES study.

INTRODUCTION

Supported bimetallic catalysts have received much attention over the last few decades as a result of both academic interest and their widespread use as catalysts in many industrial processes (1). One example of these is platinum-based catalysts for the reforming of hydrocarbons. During use, periodic regeneration, which involves removal of coke deposits and redispersion of the metallic function, is required. Coke removal is achieved by controlled oxidation, while the redispersion process involves thermal treatment under oxidizing conditions in the presence of a chlorine-containing reagent. This may also restore the acid function of the catalyst. The oxychlorination process for the monometallic platinum catalyst has been well studied and much detailed information exists regarding the redispersion mechanism and the final state of the catalyst (2–7). However, current reforming catalysts contain rhenium or tin to suppress undesired side reactions and enhance performance between regeneration stages. Many studies have been performed in which the degree of interaction between the two components in their fresh state has been assessed and a degree of controversy still exists as to whether Pt and Re are fully alloyed or not and whether the Re is completely reduced (8–18). Regarding the mechanism of reduction, debate continues as to whether this proceeds via partially hydrated mobile Re species (8, 11, 17) or via spillover hydrogen from platinum (9). Additionally, and unlike the case of the monometallic catalyst, little attention (1, 19) has been focused on the oxychlorination–redispersion process where two metals are involved and to the state of the catalyst after regeneration procedures. Of particular interest is the state of the components after oxychlorination, their distribution on the support with respect to each other, and how the regeneration procedure affects the distribution of the two components on the surface of the final active catalyst in its reduced state.

It has been shown that by combining factor analysis with X-ray absorption near-edge structure (XANES) experiments, it is possible to extract the number and identity of the phases present during thermal treatments of catalysts, for example, during temperature-programmed reduction (TPR)-type experiments (20–23) and catalytic reaction studies (24–26). XANES (27) and XANES–TPR-type experiments (28–30) have been performed for fresh Pt–Re catalysts, and the importance of maintaining Cl levels after any precalcination step has been emphasized (30). Although the role of mobile chloride-containing Pt species in the redispersion process is well established (2–7), the formation of rhenium oxychlorides has not been proven (30). By preparing catalyst using chloride-free precursors, the current objectives were to perform reduction and oxychlorination cycles and determine the nature of chlorine-containing species formed during oxychlorination and their role in the reduction and alloying process. An additional aim was to discern whether the nature of these phases

[1] To whom correspondence should be addressed. E-mail: ICPMF03@PINAR1.CSIC.ES.

0021-9517/99 $30.00

changes after successive cycles (i.e., more/less alloying, formation of more stable, unreducible metal chlorides, etc.). The effect of similar consecutive cycles of treatments has been investigated for monometallic platinum catalysts (5, 31) and the results were summarized in a recent review (32).

EXPERIMENTAL

Catalyst Preparation

A 0.3 wt% Pt catalyst was prepared by wet impregnation of Degussa-C γ-alumina using tetraammineplatinum(II) hydroxide (Johnston Matthey-Alfa). The catalyst was dried at 383 K prior to storage. A quantity of this sample was calcined in flowing air at 673 K for 1 h prior to the addition of an amount of 1.48% stock solution of Re salt prepared from rhenium heptoxide (Johnston Matthey-Alfa), calculated to provide 0.3 wt% Re. The sample was also dried at 383 K prior to storage.

An additional bimetallic catalyst was prepared for comparative purposes in which both precursors, using the same salts and concentrations as for the stepwise prepared catalyst, were added in a single stage prior to drying at 383 K.

Catalyst Treatments

Chemisorption and reaction studies were carried out in the same reactor vessel using identical pretreatment procedures as follows. Sample was heated at 15 K min^{-1} to 673 K in flowing air (60 cm^3 min^{-1}) before isothermal treatment for 1 h at 673 K. The reactor was then purged with N_2 before heating to the reduction temperature (773 K) in flowing H_2. This temperature was held for 1 h before cooling to reaction temperature (623 K) or to the temperature of chemisorption (298 K). Subsequent cycles involved heating to 823 K in flowing air and maintaining this temperature for 1 h. During this isothermal period, 1,2-dichloropropane (DCP) was injected at the rate of 30 μl h^{-1} which was reduced to 15 μl h^{-1} for subsequent cycles. Following oxychlorination, the sample was reduced at 773 K as above prior to chemisorption or reaction studies.

Catalysts used in XANES experiments were calcined *ex situ* at 673 K followed by quick transfer to the XANES cell and purging with He at 423 K for 60 min, followed by reduction in flowing 5% H_2/He by raising the temperature from 423 to 773 K at 7 K min^{-1}. The sample was held at 773 K for 15 min before cooling under He to 623 K where it was held for 60 min. Oxychlorination of the sample was performed in a 6.8 K min^{-1} ramp from 623 to 823 K followed by a 30-min isothermal period at 823 K. Air (45 cm^3 min^{-1}) and a blend of 1270 ppm DCP in He were used to deliver 1 wt% Cl to the sample during the treatment. The flow of DCP in He was reduced by half for subsequent cycles. Following oxychlorination, the sample was cooled to 423 K in pure He prior to the next reduction. This series of treatments was repeated for up to three cycles. A less extended series of cycles (up to two) were performed on a sample that was calcined *in situ* at 673 K.

XANES Measurements and Computational Details

XANES experiments at the Re and Pt L_{III} edges were performed on line CII at the Cornell High Energy Synchrotron Source. A Si(111) double-crystal monochromator was used with 50% detuning to minimize harmonic content of the beam. Transmission experiments were carried out using N_2-filled ionization chambers for detection. The energy scale was calibrated by simultaneously measuring the corresponding metal foil using a third ionization chamber filled with Ar. Samples were presented in the form of self-supporting wafers (absorbance of 1.5–1.8) and placed in a controlled-atmosphere cell for cycling treatment as described above.

The XANES spectra collected during reduction and oxychlorination treatments were analyzed using principal-component factor analysis (PCA), (20, 26). The PCA assumes that the absorbance in a set of spectra can be mathematically modeled as a linear sum of individual components, called factors, which correspond to each one of the metal species present in a sample, plus noise (33). To determine the number of individual components, an F test of the variance associated with factor k and the summed variance associated with the pool of noise factors is performed. A factor is accepted as a "pure" species (factor associated with signal and not noise) when the percentage of significance level of the F test, % SL, is lower than a test level set in previous studies at 5% (20–26). The ratio between the reduced eigenvalues, $R(r)$, which must approach one for noise factors, is also used in reaching this decision. Once the number of individual components is set, XANES spectra corresponding to individual platinum or rhenium species and their concentration profiles are generated by an orthogonal rotation (varimax rotation) which should align factors (as close as possible) along the unknown concentration profiles, followed by iterative transformation factor analysis (ITFA). ITFA starts with delta function representations of the concentration profiles located at temperatures predicted by the varimax rotation, which are then subjected to refinement by iteration until error in the resulting concentration profiles is lower than the statistical error extracted from the set of raw spectra (20, 26). XANES-based simulations related with hydrogen consumption during reduction were obtained from the derivative of the concentration profiles for oxidized species (e.g., Pt^{4+} and Re^{7+}) present along the reduction coordinate. An intermediate compound concentration profile detected in the Re edge is also considered to account for metal transformation and hydrogen consumption by the sample.

n-Heptane Reforming

Reforming of *n*-heptane was performed at 623 K at atmospheric pressure in a vertically mounted, fixed-bed reactor of 9.7-mm internal diameter. Fifty milligrams catalysts in the mesh range 210–300 μm was located on a quartz frit to produce a 1-mm-high catalyst bed with a quartz wool plug above the catalyst, allowing preheating of the feed stream. Heating was achieved by an external furnace controlled by a calibrated variac supply while a thermocouple located within a quarzt tube, positioned within the catalyst bed, provided temperature monitoring. A 10 : 1 molar ratio of H_2 : heptane was used at a GHSV of 2030 h^{-1}. Under these conditions, heptane conversion was below 10%. In addition to the oxychlorination/reduction cycle experiments reported here, oxidation/reduction cycles that involved the same initial calcination/reduction treatment were also performed. The repetition of this treatment and subsequent reaction over identically treated catalyst, allows for a high degree of confidence with respect to the reproducibility of the experimental results obtained. Analysis of reaction products involved an on-line Perkin–Elmer 8410 gas chromatograph fitted with a flame ionization detector and a 5.6 m column containing 15% squalane on Chromosorb W-HP (80-100 mesh).

Dispersion Measurements

The dispersion of Pt was measured for samples treated as outlined above followed by cooling to 298 K in flowing N_2, introduction of a succession of 0.364-μmol pulses of H_2 into the carrier gas, with the sample at 298 K, and measurement of the proportion of consumed H_2 using a thermal conductivity detector fitted to a Perkin–Elmer Autosystem XL gas chromatograph.

RESULTS

Table 1 summarizes dispersion measurements based on hydrogen chemisorption for Pt-only and Pt–Re catalysts after an initial calcination–reduction cycle and then subsequent oxychlorination/reduction cycles. The monometallic catalyst initially shows a dispersion of 50%, somewhat lower than a similar 0.3% loaded EUROPT-3 catalyst (34). Unlike previous studies (6), hydrogen rather than CO was chosen as adsorbate to measure Pt surface fraction as prolonged exposure of the latter to the Re-containing samples used here led to formation of rhenium multicarbonyls of varying stoichiometry (35). Hydrogen chemisorption under conditions used here may be assumed to selectively measure the number of exposed Pt atoms (36). Table 1 shows that the initial hydrogen consumption of the bimetallic catalyst is lower than for monometallic Pt, although again cycles of oxychlorination/reduction led to enhanced uptakes. Further subsequent treatments of up to six oxychlorination/reduction cycles failed to increase this H/Pt ratio beyond ca. 0.24 (37).

TABLE 1

Hydrogen Chemisorption

Treatment	H : Pt	
	Pt/Al_2O_3	$Pt–Re/Al_2O_3$
Calcination/reduction	0.51	0.16
First oxychlorination/reduction	0.68	0.245
Second oxychlorination/reduction	0.69	0.21

TABLE 2

Re L_{III}-Edge Principal-Component Factor Analysis Results for the Bimetallic Sample

Factor	Eigenvalue	% SL	$R(r)$	Variance[a]
	(a) First reduction			
1	1080.921	0.00	29.43	96.956
2	33.6932	0.00	177.24	2.982
3	0.17364	0.28	5.60	0.014
4	0.02806	8.44	2.04	0.002
5	0.01238	17.59	1.66	
6	0.00664	27.17	1.05	
7	0.00560	26.57	1.33	
8	0.00366	32.91	1.11	
	(b) Second reduction			
1	1015.92	0.00	187.45	99.506
2	4.98582	0.00	133.26	0.489
3	0.03416	0.92	4.89	0.003
4	0.00632	14.79	1.17	0.001
5	0.00486	13.07	2.04	
6	0.00212	26.09	1.15	
7	0.00163	27.91	0.96	
8	0.00147	24.68	1.44	

[a] Variance is expressed as a percentage. Values lower than 10^{-3} are not reported.

Tables 2a and 3a show factor analysis/XANES results for the bimetallic sample, giving evidence for the existence of three Re and two Pt species during the first reduction treatment. At both edges, only one oxidized (No. 1 in Figs. 1 and 2) and one reduced (No. 3 in Fig. 1 and No. 2 in Fig. 2) species are observed. The Re edge also shows evidence of an intermediate compound, species 2 (Fig. 1), formed during the reduction process. The corresponding concentration profiles can be seen in Fig. 3 along with the derivative of concentration profiles for the oxidized and intermediate species. These derivative curves indicate that Pt is reduced in two stages (515 and 582 K) while Re has a two-step reduction mechanism with a first prominent peak at 572 K and a second, broad contribution ranging from 625 to 800 K. During the first oxychlorination, only one species is detected in the Re edge while two are observed for Pt (Table 3b). Initial contact with the DCP/air mixture at 623 K reverts Re to its initial state (compare species 1 and 1′ in Fig. 1),

TABLE 3

Pt L_{III}-Edge Principal-Component Factor Analysis Results for the Bimetallic Sample

Factor	Eigenvalue	% SL	$R(r)$	Variance[a]
	(a) First reduction			
1	489.902	0.00	73.85	99.781
2	5.97234	0.00	242.32	0.204
3	0.02206	21.88	1.22	0.004
4	0.01595	23.91	1.52	0.004
5	0.00915	33.20	1.11	0.001
6	0.00707	36.27	1.08	0.002
7	0.00552	39.48	0.88	0.001
8	0.00514	37.74	1.09	0.001
	(b) First oxychlorination			
1	537.982	0.00	685.43	99.855
2	0.70882	0.00	25.45	0.132
3	0.02495	16.22	2.03	0.005
4	0.01087	30.79	1.23	0.002
5	0.00774	36.07	0.95	0.001
6	0.00701	35.38	1.14	0.001
7	0.00516	40.13	0.99	0.001
8	0.00425	42.65	0.84	0.001
	(c) Second reduction			
1	597.613	0.00	484.234	99.799
2	1.12652	0.00	51.23	0.188
3	0.01995	20.22	1.55	0.004
4	0.01160	29.21	1.05	0.002
5	0.00983	29.74	1.19	0.001
6	0.00728	33.94	1.28	0.002
7	0.00497	41.10	0.93	
8	0.00459	41.32	0.95	

[a] Variance is expressed as a percentage. Values lower than 10^{-3} are not reported.

with this species remaining throughout the treatment. On the other hand, the Pt edge shows one species that is distinct from the initial species detected during the first reduction and that is slowly transformed into a compound with local order similar to that of PtO_2. The corresponding concentration profiles (not shown for the sake of brevity) show a small contribution around 645 K and a broad, larger maximum centered at 745 K. The second reduction roughly parallels the first, with the same number of oxidized, intermediate, and reduced compounds (Tables 2b and 3c) but with several important differences with respect to fine details. First, the Re intermediate and reduced compounds present different edge energies. Second, Pt and Re species are reduced over wider temperature ranges (Fig. 4), showing several maxima located at 503, 548, and 636 K for Pt and 516, 576, and 623 K for Re. XANES results for subsequent reduction/oxychlorination cycles are omitted due to their similarity with results for the second reduction and first oxychlorination treatments.

X-ray absoption experiments were also conducted using a sample prepared by simultaneous impregnation of the

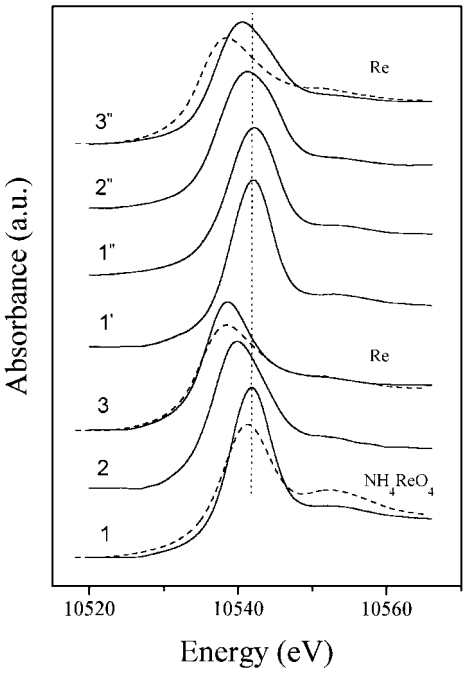

FIG. 1. Predicted pure Re components of the 0.3 wt% Pt–0.3 wt% Re/Al_2O_3 catalyst obtained during the first reduction (unprimed), first oxychlorination (primed), and second reduction (double-primed) treatments. Spectra indicated by the dashed lines correspond to the reference materials given in the figure.

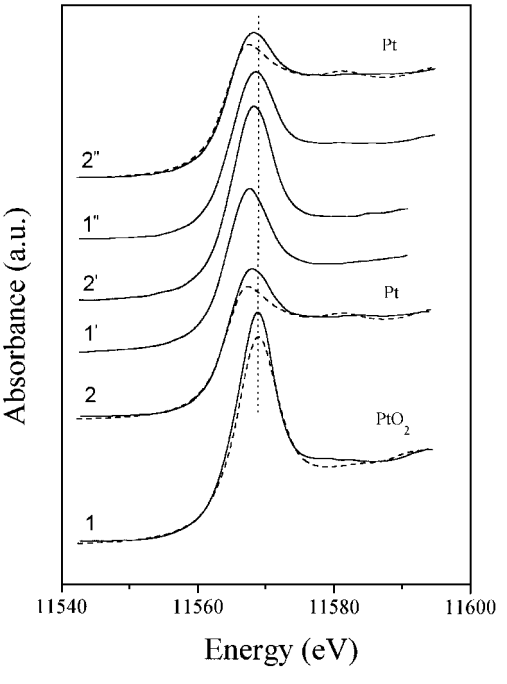

FIG. 2. Predicted pure Pt components of the 0.3 wt% Pt–0.3 wt% Re/Al_2O_3 catalyst obtained during the first reduction (unprimed), first oxychlorination (primed), and second reduction (double-primed) treatments. Spectra indicated by the dashed lines correspond to the reference materials given in the figure.

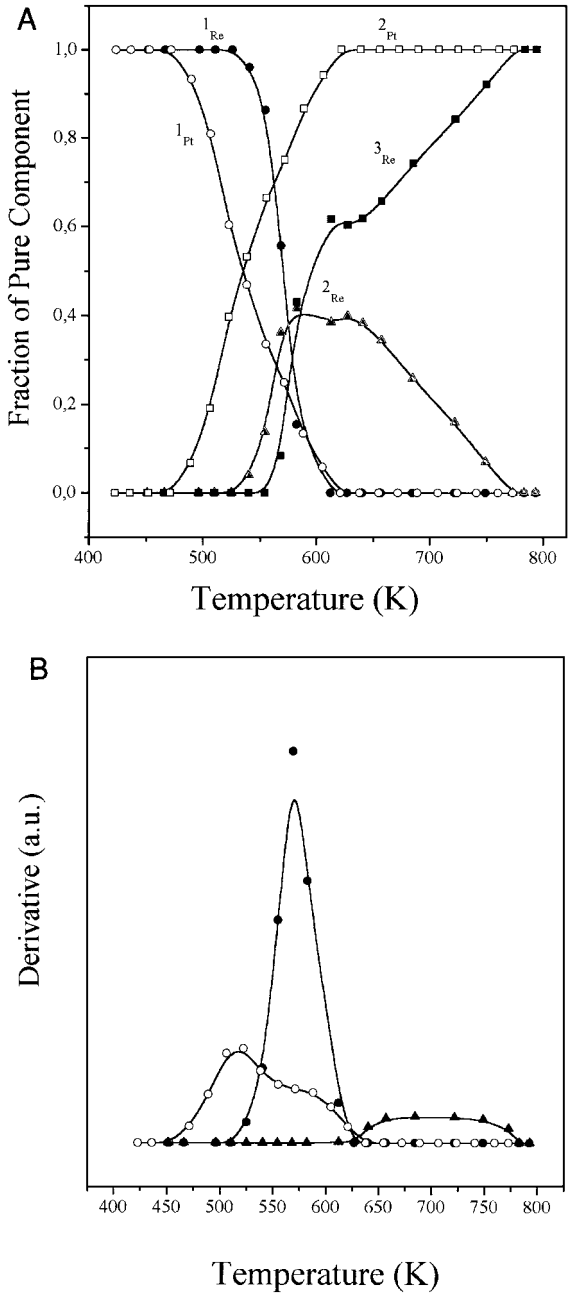

FIG. 3. (a) Re (full symbols) and Pt (open symbols) concentration profiles during first reduction. Concentration profiles are labeled following the notation used in Figs. 1 and 2. (b) Derivative of the concentration profiles. See text for details.

Pt and Re precursors as well as with an *in situ* calcined portion of the stepwise one; however, no significant differences among the corresponding XANES sets of raw spectra were apparent. This fact, on the other hand, reinforces our confidence in the X-ray absorption results outlined. Experiments conducted following the same procedure using a sample of 0.3% Re/Al_2O_3 showed no edge shift nor reduction in white line intensity, indicating that Re in the absence of platinum is, as expected, not significantly reduced under these conditions.

Table 4 shows product selectivities from *n*-heptane reforming over the mono- and bimetallic samples subjected to similar treatment cycles. Both catalysts, irrespective of pretreatment, experienced a gradual loss in activity over the 8-h period during which measurements were performed, which can be attributed to poisoning due to formation of carbonaceous layers. To extract information relating to the

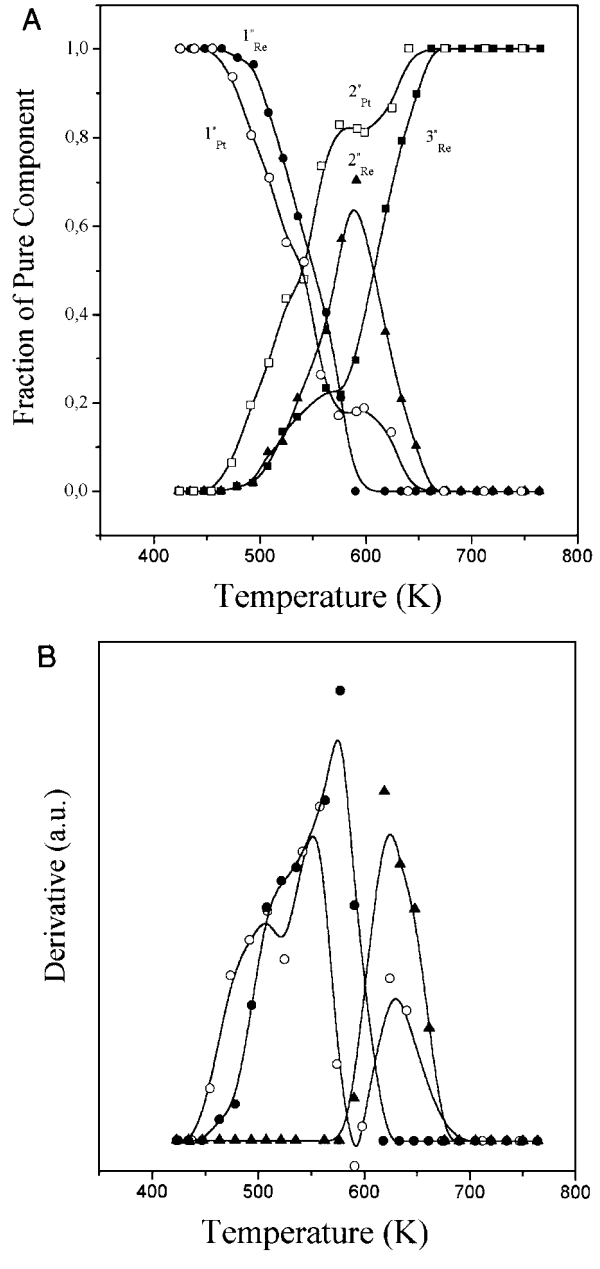

FIG. 4. (a) Re (full symbols) and Pt (open symbols) concentration profiles during second reduction. Concentration profiles are labeled following the notation used in Figs. 1 and 2. (b) Derivative of the concentration profiles. See text for details.

TABLE 4

Initial Product Selectivities in *n*-Heptane Reforming

Treatment	Aromatization	Cyclization	Isomerization	Hydrogenolysis
		Pt/Al_2O_3		
Calcination/reduction	21.07	24.65	21.86	32.42
First oxychlorination/reduction	23.62	22.14	21.51	32.73
Second oxychlorination/reduction	23.12	21.95	21.38	33.56
		$Pt–Re/Al_2O_3$		
Calcination/reduction	12.57	19.12	12.71	55.60
First oxychlorination/reduction	9.47	12.25	10.04	67.24
Second oxychlorination/reduction	7.39	12.30	10.51	69.81

metallic content of the surface layers, selectivities have been compared for samples immediately after exposure to *n*-heptane when the amount of carbonaceous laydown is small. Monometallic catalyst shows results that are reasonably well distributed in terms of the four categories of reaction products. Despite increased dispersion following subsequent oxychlorination/reduction cycles (Table 1), selectivities to the various types of reaction product remained unaffected (Table 4). Re-containing catalysts after calcination–reduction show selectivities indicating increased levels of hydrogenolysis, largely at the expense of aromatization and isomerization products.

DISCUSSION

After calcination, there is no evidence of interaction between the two components of the Pt–Re system. While Pt is located in small particles with local order similar to that found in PtO_2, Re is present in an oxidation state close to Re^{7+}. The difference in the white line intensity and edge position with the NH_4ReO_4 reference, in which the local symmetry is tetrahedral, is due to the lack of large or three-dimensional order. Differences exhibited between XANES of solid and liquid ammonium perrhenate (29) are consistent with this interpretation. IR studies indicate that Re species on hydrated alumina surfaces are indistinguishable from aqueous $(ReO_4)^-$ units (30). The absence of binary, oxidized phases in conjunction with the low loadings used (which do not induce severe competition for alumina surface sites) explain the moderate to low influence of the preparation procedure (coimpregnation and stepwise impregnation) in the oxychlorination/reduction treatments.

The first reduction process of the catalyst goes through a Re intermediate that is most likely a hydroxide or oxohydroxide. Assuming that the correlation between formal oxidation state and chemical shift for oxidic Re compounds (29) can be applied here, Re must be present in a Re^+ state in this species. The intensity of the white line also indicates a low oxidation state. Note, however, that for oxidic Re species, the white line intensity increases with the oxidation state only up to Re(VII) which exhibits a lower than expected value, resulting in deviation from this linear relationship (29). The reduction process is completed with Pt present in a phase that in terms of both white line intensity and energy position is clearly modified with respect to monometallic Pt. Note that differences with the Pt foil reference can, in part, be attributed to hydrogen-induced states originating from hydrogen chemisorption (38) but this alone cannot fully account for the difference in shape. The final Re species is similar to monometallic Re but with a significantly larger density of unoccupied *d* states. More importantly, the derivative (Fig. 3) of the concentration profiles (from Pt^{4+}, PtO_2, to Pt^0; Re^{7+}, $(ReO_4)^-$ units to Re^+; and Re^+ to Re^0), which can be compared with conventional H_2 consumption temperature-programmed reduction (TPR) experiments, shows a peak at 572 K that is characteristic of alloy formation (29, 30, 34). This is commonly observed for samples pretreated with He or N_2 below 573 K (30, 34). On the other hand, no sizable peak should appear in the 623–823 K range, which is often interpreted in terms of unalloyed Re (30). Note that the reduction peak between 625 and 800 K for Re (Fig. 3) indicates reduction of the intermediate, i.e., Re(1+) to Re(0) and therefore would show negligible hydrogen consumption relative to the other peaks in a conventional TPR plot [the *y* axis has not been scaled to consider relative uptakes but taking into account the Pt : Re atomic ratio of the sample and that the reducible compounds are PtO_2, $(ReO_4)^-$ units, and a Re^+ phase, the derivative curves of Fig. 3 should be multiplied by 1, 2, and 0.5, respectively, to account for hydrogen consumption]. Note, of course, that these are very rough estimations of the reduction process stoichiometries.

Summarizing the above, the results suggest that a single alloyed phase is present after reduction. This alloy exhibits a Re-like hcp local structure in which both metals suffer important electronic modification in their *d* bands with respect to their monometallic states. The local structure of the alloy can be inferred from the energy position of the continuum resonances (CRs) observed in the XANES spectra, while the ≈11,580 eV Pt resonance (species 2 in Fig. 2) is clearly shifted to higher energy (about 1.7 eV) with respect to the Pt foil, the Re CR at ≈10550 eV is largely unaffected.

Although the CR energy position is affected by electronic as well as geometric factors, the inverse dependence of the latter with the square of the coordination distance strongly suggests that the Pt-containing alloy has significantly lower average coordination distance with respect to a monometallic Pt fcc structure. Among PtRe alloys, those with Re-like hcp structure present the shorter metal–metal distances and due to the smaller atomic diameter of Re, modification of the Pt coordination distance occurs to a greater extent than for Re (39), in agreement with our experimental results. A possible influence of the (small) particle size in the coordination distance could also contribute to its decrease with respect to metallic-foil references but should similarly affect both Pt and Re components of the alloy. On the other hand, this interatomic distance decrease has been estimated to be $\approx$0.1 Å by previous X-ray absorption fine structure (EXAFS) studies, which, in addition, show some Re segregation to the bimetallic surface (40).

In brief, the XANES analysis shows that both metals do not interact significantly in the oxidized state and that reduction generates an alloy phase through a mobile Re-containing species in which the Re is present in an oxidation state close to 1+. This finding is consistent with the opinion (41) that Re oxide species are highly mobile even in the absence of chlorine for any level of alumina hydration (once that spillover hydrogen is present), as shown here (see below) by alloy formation in the first (Cl-free) and second (Cl-present) reductions. To our knowledge, this is the first direct experimental evidence for such an intermediate in the reduction of Pt–Re. The detection of such an intermediate under conditions where clear evidence exists for alloy formation is of significance as this gives considerable support to a mechanism involving Re oxide migration (8, 11, 17) rather than hydrogen spillover from zero-valent Pt particles to initiate the autocatalytic reduction of Re (9) which would leave the respective metals in their isolated, unalloyed states. However, Re reduction always follows the onset of Pt reduction, indicating that spillover hydrogen is required to generate the mobile Re species, although contrary to opinion (8, 11, 17), this mobile species is in a partially reduced rather that a fully oxidized state. It should be stressed that although the maximum rate of hydrogen consumption is ca. 573 K, in agreement with other reports (29, 30, 34), this reflects the maximum rate of formation of the mobile Re species and not of the alloy phase which occurs at a higher temperature and without significant hydrogen consumption. The final alloyed phase develops above 550 K and has a hcp Re-like (local) structure, a fact of some significance when considering several aspects of the Pt–Re system, e.g., whether the decrease in hydrogen chemisorption between mono- and bimetallic samples is related to the degree of alloy formation or to Pt dispersion (34).

After the initial reduction, oxychlorination reverts the Re to its VII oxidation state, in agreement with TPR studies (10) which show that oxidation temperatures between 623 and 673 K are required for this degree of reoxidation. Following oxychlorination at 623 K, Pt presents a spectrum ascribable to an oxychloride species. This last assignment is based on the shift to lower energy of the white line, with respect to species 1 in Fig. 2, which is characteristic of the Pt chloride references (not shown) and clearly indicates the presence of ligands such as Cl^- with a Pt–L coordination distance greater than that corresponding to O^{2-}. The density of unoccupied *d* states is also significantly lower in Pt chlorides than Pt oxides, as indicated by spectra of species 1′ and 1 in Fig. 2. The initial coordination sphere of Pt most likely contains both oxygen and chlorine ligands, consistent with the general view (2–7, 30) that platinum oxychloride species are produced during the oxychlorination treatment. The Cl^- anions are eventually lost as the temperature approaches 823 K, finally generating a Pt species with coordination similar to that found in PtO_2. Therefore, the redispersion stage appears to initially disrupt the alloy particles (623 K), yielding Re oxide and Pt oxychloride clusters, before final decomposition of the latter to yield an exclusively oxidic environment. Wagstaff and Prins (10) report that treatment of reduced Pt–Re catalysts with oxygen above 473 K results in segregation into the component oxides. During oxychlorination, chlorine anions selectively interact with the Pt (and alumina) without affecting the Re component of the bimetallic phase. Michel *et al.* (30) believe that in the absence of water, mobile Re oxychloride species must be formed, although the only mobile Re phase detected here is a Re(1+) oxide or oxohydroxide which is present during the reduction stages.

The presence of chlorine anions in the system, mainly those retained by the alumina, has, however, important consequences for subsequent reduction treatments. In particular, the Re–chloride interaction, absent during the oxychlorination treatment, will be shown to play a role in determining the chemical and catalytic properties of the bimetallic phase that is formed. The second reduction (Fig. 4) starts at a relatively lower temperature and proceeds over a wider range than the first. Pt again initiates the process but is closely followed by Re. The differences compared with the first reduction can be explained by considering that the oxychlorination treatment induces a certain heterogeneity in the particle size distributions and changes in the mobility of the Re intermediate. Isaacs and Petersen (11) report that TPR peaks for Pt–Re become significantly broader for higher (773 K) calcination temperatures while Wagstaff and Prins (10) report that reoxidation of reduced catalysts at temperatures below 673 K enhances Pt reducibility whereas reoxidation above 773 K shifts the TPR peaks to higher temperatures. It appears that there are some metal oxide particles that interact weakly with the alumina and are reduced at lower temperatures than in the first reduction and a part of the

Pt that interacts strongly with the support, possibly resulting from the presence of Cl in the vicinity generated by decomposition of the oxychloride, which is reduced around 635 K. The last comment is consistent with the fact that Cl-free Pt samples are generally reduced around 393 K (8) while samples produced from Cl-containing precursors are normally reduced around 573 K (9, 10, 11, 17). Despite the absence of a clear physical model for the Re environment of the intermediate and reduced species after the second reduction, some indications can be inferred from the XANES spectra. First, a Cl–Re interaction could justify the edge shift observed, as chlorine environments always produce Re edges at higher energies than oxidic environments (42, 43). The increased heterogeneity of the Re environment from the first to second reduction is also manifested in the greater FWHM of the white line. These facts suggest that the mobilization process of Re may induce contact with Cl^- anions previously adsorbed on the support, somehow subtlety affecting the mechanics of the alloying process and favoring the presence of electronically modified Re atoms at the surface of the final zero-valent particles. The formation of particles with a Pt-rich core is consistent with the fine details in the Pt L_{III}-edge data. The zero-valent species obtained after the second reduction (species 2″ in Fig. 2) exhibits a CR at ≈11,580 eV, perturbed by only 0.4 eV with respect to the Pt foil and shows a greater degree of correlation with the white line intensity of the foil compared with the Pt species present after the first reduction. This would indicate a more monometallic Pt-like fcc environment after the second reduction than after the first reduction. Following the second reduction, the metal particles can be envisaged as being composed of a fcc Pt-rich core, covered with a Re-rich surface. This would be consistent with results for higher-loaded catalysts where Re is thought to grow epitaxially over a Pt core forming an fcc structure (44). The Re atoms at the surface sense the presence of chlorine anions although the scope and consequences of the Re–Cl interaction cannot be established with the present data. However, in the absence of water, chlorine plays a role clearly different from the formation of Re oxychlorides during oxychlorination treatments and connected with the modification of the alloying process during subsequent reductions.

The formation of Pt–Re alloy is consistent with catalytic measurements (Table 4) where Re is known to exhibit a higher inherent activity for hydrogenolysis (45, 46) and has been considered as a characteristic of Pt–Re alloy formation in unsulfided catalysts (47). The presence of Re at the surface of the bimetallic particles after the first reduction and the important Re surface enrichment suggested by XANES measurements after the second reduction would be then consistent with the enhanced hydrogenolysis selectivity trend observed in going from Pt to Pt–Re catalysts and from the first to second cycle in the binary system. The subsequent surface Re-support contact has also been detected by EXAFS through a Re–O^{2-} contribution and considered to stabilize metal dispersion during reaction (40). On the other hand, the decrease in hydrogen chemisorption observed (Table 1) has been used as evidence of alloy formation (34) and attributed primarily to a decrease in the number of contiguous Pt atoms, although a modification of the adsorption properties of Pt atoms in a hcp structure with respect to a monometallic fcc structure may also contribute to this behavior. The surface enrichment by Re going from first to second reduction cycles might therefore be expected to lead to further decreases in hydrogen uptake, contrary to findings (Table 1); however, the total uptake will reflect a complex balance between overall metal dispersion, surface composition, and chemical characteristics of the different (hcp vs fcc) Pt phases. In a previous study (34), the extent of hydrogen chemisorption and selectivity to hydrogenolysis during *n*-heptane conversion was used to describe the extent to which Pt and Re alloy formation occurs and this was related to the degree of mobility in the presence or absence of Cl. Results here suggest that both observations can be attributed, at least partly, to differences in the distribution of the active components within the bimetallic particles.

Subsequent oxychlorination/reduction cycles produced only very slight changes in the bimetallic sample chemical characteristics (hydrogen chemisorption or *n*-heptane reaction) and very similar XANES results, giving evidence that the most dramatic effect of cycling treatments occurs during the first and second cycles.

CONCLUSIONS

XANES studies of a Pt–Re/Al_2O_3 catalyst subjected to oxychlorination/reduction cycles indicate a reduction mechanism that proceeds through a Re(I) intermediate, possibly an oxohydroxide, leading to complete alloying of both components. This alloy species formed after the first reduction has a hcp Re-like structure with electronic modification of Re and Pt with respect to their single, metallic state. Oxychlorination of the sample proceeds via selective interaction of Cl with Pt, disrupting the alloy particles. No evidence of a Re oxychloride species was obtained, although indirect evidence of interactions between the chloride and Re in the mobile species and in the reduced bimetallic particles was suggested by the results. The amount of chlorine in contact with Pt is a function of the treatment temperature, decreasing at higher oxychlorination temperatures. At 823 K, the final result is redispersion of both active components into their single, monometallic oxides. Subsequent reduction leads to reformation of a Pt–Re alloy but with clear differences in both physical (i.e., particle size and local order) and chemical (i.e., active metal distribution within the alloy particle and surface composition) properties compared with the first reduction. This is attributed to the combined effect of the oxidized particle

size distributions obtained after oxychlorination and to the presence of chloride (attached to the support) interactions with reduced Re states, which leads to this metal predominating at the surface of the binary zero-valent fcc-structured particles. The XANES characterization is supported by results for hydrogen chemisorption and *n*-heptane reforming obtained after successive treatment cycles.

ACKNOWLEDGMENTS

We thank the Royal Society (London) for a University Research Fellowship (J.A.A), the Royal Society of Chemistry for a J. W. T Jones Travelling Fellowship (J.A.A.), the CSIC (Spain) for a Postdoctoral Contract (M.F.G.), and the Malaysian Goverment and Universiti Putra for a postgraduate scholarship (F.K.C.). Research carried out at Cornell High Energy Synchrotron Source (CHESS) was supported by the National Science Foundation.

REFERENCES

1. Ponec, V., and Bond, G. C., *Stud. Surf. Sci. Catal.* **95**, 583 (1995).
2. Frank, J. P., and Martino, G. P., *in* "Progress in Catalyst Deactivation" (J. L. Figueiredo, Ed.), p. 355. Nijhoff, The Hague, 1982.
3. Lee, T. J., and Kim, Y. G., *J. Catal.* **90**, 279 (1984).
4. Foger, K., and Jaeger, H., *J. Catal.* **92**, 64 (1985).
5. Lieske, H., Lietz, G., Spindler, H., and Völter, J., *J. Catal.* **81**, 817 (1983).
6. Anderson, J. A., Mordente, M. G. V., and Rochester, C. H., *J. Chem. Soc. Faraday Trans.* **85**, 2983, 2991 (1989).
7. Beltramini, J. N., *in* "Catalytic Naptha Reforming" (G. J. Antos, A. M. Aitani, and J. M. Parera, Eds.), p. 313. Marcel Dekker, New York, 1995.
8. Augustine, S. M., and Sachtler, W. M. H., *J. Catal.* **116**, 184 (1989).
9. Mieville, R. L., *J. Catal.* **87**, 437 (1984).
10. Wagstaff, N., and Prins, R., *J. Catal.* **59**, 434 (1979).
11. Isaacs, B. H., and Peterson, E. E., *J. Catal.* **77**, 43 (1982).
12. Leclercq, G., Charcosset, H., Maurel, R., Bertizeeau, C., Bolivar, C., Frety, R., Jaunay, D., Mendez, H., and Tournayan, L., *Bull. Chem. Soc. Chim. Belg.* **88**, 577 (1979).
13. Peri, J. B., *J. Catal.* **52**, 144 (1978).
14. Kelley, M. J., Freed, R. L., and Swartzfarger, D. G., *J. Catal.* **78**, 445 (1982).
15. Huang, Z., Fryer, J. R., Park, C., Stirling, D., and Webb, G., *J. Catal.* **148**, 478 (1994).
16. Wang, L., and Hall, W. K., *J. Catal.* **82**, 177 (1983).
17. McNicoll, B. D., *J. Catal.* **46**, 438 (1977).
18. Johnson, M. F. L., and LeRoy, V. M., *J. Catal.* **35**, 434 (1974).
19. Parera, J. M., and Figoli, N. S., "Specialist Periodical Reports—Catalysis," Vol. 9, p. 65. Roy. Soc. of Chem., London, 1992.
20. Fernández-García, M., Márquez-Alvarez, C., and Haller, G. L., *J. Phys. Chem.* **99**, 12565 (1995).
21. Fernández-García, M., Anderson, J. A., and Haller, G. L., *J. Phys. Chem.* **100**, 16247 (1996).
22. Ferreira-Aparicio, P., Bachiller-Baeza, B., Rodríguez-Ramos, I., Guerrero-Ruiz, A., and Fernández-García, M., *Catal. Lett.* **35**, 163 (1997).
23. Fernández-García, M., Rodríguez-Ramos, I., Ferreira-Aparicio, P., and Guerrero-Ruiz, A., *J. Catal.* **178**, 253 (1998).
24. Fernández-García, M., Márquez-Alvarez, C., Rodríguez-Ramos, I., Guerrero-Ruiz, A., and Haller, G. L., *J. Phys. Chem.* **99**, 16380 (1995).
25. Anderson, J. A., Fernandez-Garcia, M., and Haller, G. L., *J. Catal.* **164**, 477 (1996).
26. Márquez-Alvarez, C., Rodríguez-Ramos, I., Guerrero-Ruiz, A., Haller, G. L., and Fernandez-García, M., *J. Am. Chem. Soc.* **119**, 2905 (1997).
27. Onuferko, J. H., Short, D. R., and Kelley, M. J., *Appl. Surf. Sci.* **19**, 227 (1984).
28. Michel, C. G., Bambrick, W. E., Ebel, R. H., Larson, G., and Haller, G. L., *J. Catal.* **154**, 222 (1995).
29. Hilbrig, F., Michel, C. G., and Haller, G. L., *J. Phys. Chem.* **96**, 9893 (1992).
30. Michel, C. G., Bambrick, W. E., and Ebel, R. H., *Fuel Proc. Tech.* **35**, 159 (1993).
31. Mordente, M. G. V., and Rochester, C. H., *J. Chem. Soc. Faraday Trans.* **85**, 3495 (1989).
32. Dadyburjor, D. B., "Specialist Periodical Reports—Catalysis," Vol. 9, p. 229. Roy. Soc. of Chem., London, 1992.
33. Malinoswki, E. R., "Factor Analysis in Chemistry." Wiley, New York, 1991.
34. Presvik, R., Moljord, K., Grande, K., and Holmen, A., *J. Catal.* **174**, 119 (1998).
35. Anderson, J. A., Chong, F. K., and Rochester, C. H., *J. Mol. Catal.*, in press.
36. Bolivar, C., Charcosset, H., Frety, R., Primet, M., Tournayan, L., Betizeau, C., Leclercq, G., and Maurel, R., *J. Catal.* **45**, 163 (1976).
37. Anderson, J. A., Chong, F. K., and Rochester, C. H., to be published.
38. Ichikuni, N., and Iwasaka, Y., *Catal. Lett.* **20**, 87 (1993).
39. Trzebiatowski, W., and Berak, J., *Bull. Acad. Pol. Sci. II*, 37 (1954).
40. Via, G. H., and Sinfelt, J. H., *in* "X-Ray Absorption Fine Structure for Catalysts and Surfaces" (De. Y. Iwasawa, Ed.), pp. 168, 169. World Scientific, Singapore, 1996.
41. Malet, P., Munuera, G., and Caballero, A., *J. Catal.* **115**, 567 (1989).
42. Shapiro, E. S., Araev, V. I., Antonin, G. V., and Ryashentseva, M. A., *J. Catal.* **55**, 402 (1978).
43. Kirlin, P. S., Strohmeier, B. R., and Gates, B. C., *J. Catal.* **98**, 308 (1986).
44. Liang, K. S., Chien, F. Z., Hughes, G. J., Meitzner, G. D., and Sinfelt, J. H., *J. Phys. Chem.* **95**, 9974 (1991).
45. Parera, J. M., Beltramini, J. N., Querini, C. A., Martinelli, E. E., Churin, E. J., Aloe, P. E., and Figoli, N. S., *J. Catal.* **99**, 39 (1986).
46. Murthy, K. R., Sharma, N., and George, N., *in* "Catalytic Naptha Reforming" (G. J. Antos, A. M. Aitani, and J. M. Parera, Eds.), p. 313. Marcel Dekker, New York, 1995.
47. Shum, V. K., Butt, J. B., and Sachtler, W. M. H., *J. Catal.* **99**, 126 (1986).